Carolina Sarto, Sebastián Florez-Rueda, Mehrnoosh Arrar, Christian P.R. Hackenberger*, Daniel Lauster* and Santiago Di Lella*

Atomistic insight into the essential binding event of ACE2-derived peptides to the SARS-CoV-2 spike protein

https://doi.org/10.1515/hsz-2021-0426
Received November 22, 2021; accepted February 21, 2022; published online March 31, 2022

Abstract: The pathogenic agent of the severe acute respiratory syndrome coronavirus 2 (SARS-CoV-2) enters into human cells through the interaction between the receptor binding domain (RBD) of its spike glycoprotein and the angiotensin-converting enzyme 2 (ACE2) receptor. Efforts have been made towards finding antivirals that block this interaction, therefore preventing infection. Here, we determined the binding affinity of ACE2-derived peptides to the RBD of SARS-CoV-2 experimentally and performed MD simulations in order to understand key characteristics of their interaction. One of the peptides, p6, binds to the RBD of SARS-CoV-2 with nM affinity. Although the ACE2-derived peptides retain conformational flexibility when bound to SARS-CoV-2 RBD, we identified residues T27 and K353 as critical anchors mediating the interaction. New ACE2-derived peptides were developed based on the p6-RBD interface analysis and expecting the native conformation of the ACE2 to be maintained. Furthermore, we found a correlation between the helicity in trifluoroethanol and the binding affinity to RBD of the new peptides. Under the hypothesis that the conservation of peptide secondary structure is decisive to the binding affinity, we developed a cyclized version of p6 which had more helicity than p6 and approximately half of its K_D value.

Keywords: antivirals; COVID-19; inhibitors; molecular dynamics; MST; RBD.

Introduction

In the recent COVID-19 pandemic, the importance of designing neutralizing strategies for the SARS-CoV-2 virus and emerging variants has become evident. The spike protein S is the most abundant protein on the viral surface (Zhou et al. 2020). During viral infection, the spike protein is responsible for the host cell entry by first binding to angiotensin converting enzyme 2 (ACE2) (Hoffmann et al. 2020; Wang et al. 2020a; Zhao et al. 2020). Upon endocytic uptake, the spike protein triggers fusion of viral and endosomal membranes, thus releasing the viral genome into the cytoplasm, where virus replication takes place (Dodero-Rojas et al. 2021; Fan et al. 2020).

The spike protein consists of a homotrimeric structure anchored to the viral membrane by a transmembrane domain. Each monomer comprises two functional subunits, termed S1- and S2-domain. The S1-domain is responsible for the attachment to ACE2 on host cells of human airway epithelium and S2-domain mediates membrane fusion. The virus interaction with ACE2 specifically involves attachment via the receptor-binding domain (RBD) of the S1 subunit (Wang et al. 2020a). Affinity values reported for ACE2-binding to the RBD vary considerably (Kirchdoerfer et al. 2018; Nguyen et al. 2020; Walls et al. 2020; Wrapp et al. 2020). However, it is clear that SARS-CoV-2 binds ACE2 with higher

Carolina Sarto and Sebastian Florez Rueda contributed equally to this work.

***Corresponding authors: Christian P.R. Hackenberger**, Leibniz Forschungsinstitut für Molekulare Pharmakologie (FMP), Robert-Roessle-Strasse 10, D-13125 Berlin, Germany, E-mail: hackenbe@fmp-berlin.de; https://orcid.org/0000-0001-7457-4742; **Daniel Lauster**, Institut für Biochemie und Chemie, Freie Universität Berlin, Arnimallee 22, D-14195 Berlin, Germany, E-mail: daniel.lauster@fu-berlin.de; and **Santiago Di Lella**, Instituto de Química Biológica – Ciencias Exactas y Naturales – Conicet/Facultad de Ciencias Exactas y Naturales, Universidad de Buenos Aires, Ciudad Universitaria, Pabellón II, 4° Piso, C1428EGA Ciudad de Buenos Aires, Argentina, E-mail: santi@qi.fcen.uba.ar
Carolina Sarto, Instituto de Química Biológica – Ciencias Exactas y Naturales – Conicet/Facultad de Ciencias Exactas y Naturales, Universidad de Buenos Aires, Ciudad Universitaria, Pabellón II, 4° Piso, C1428EGA Ciudad de Buenos Aires, Argentina, E-mail: carolinasarto@qi.fcen.uba.ar
Sebastián Florez-Rueda, Leibniz Forschungsinstitut für Molekulare Pharmakologie (FMP), Robert-Roessle-Strasse 10, D-13125 Berlin, Germany, E-mail: florez@fmp-berlin.de
Mehrnoosh Arrar, Instituto de Cálculo – Conicet/Facultad de Ciencias Exactas y Naturales, Universidad de Buenos Aires, Ciudad Universitaria, Intendente Güiraldes 2160, Pabellón II, 2° Piso, C1428EGA Ciudad de Buenos Aires, Argentina, E-mail: mehrnoosh.arrar@gmail.com

affinity than SARS-CoV-1, despite the highly conserved structure and sequence of the RBDs of SARS-CoV-1 and SARS-CoV-2 (Lan et al. 2020; Wang et al. 2020a). This difference in binding affinities, evidently due to few sequence differences between the RBDs of SARS-CoV-1 and -2 spike proteins, warrants a closer analysis of the SARS-CoV-2 RBD interactions with ACE2 in order to design effective therapeutics that can interfere in this essential binding event. Even though the recognition mechanism through the ACE2 receptor presents some differences among coronaviruses and their variants (Brielle et al. 2020; Li 2015), viral entry is achieved through this critical interaction and consequently tackling it with a competitive inhibitor would provide a potential broad therapeutic strategy (Peter and Schug 2021).

Antiviral peptides derived from ACE2 have been identified for SARS-CoV-1 through a specific analysis of the RBD with ACE2 (Han et al. 2006). Two of the promising peptides with antiviral activity for SARS-CoV-1 have been denoted p4 and p6 (Han et al. 2006). p4 comprises part of helix-1 of ACE2 (a.a. 22–44), whereas p6 comprises the same α-helical segment linked via a glycine residue to a β-hairpin (β3-β4 hairpin, a.a. 351–357 of ACE2) (Figure 1). Interestingly, p6 has a 500-fold higher antiviral activity than p4 for the SARS-CoV-1 (Han et al. 2006), indicating a substantial impact of the slight extension of the peptide to include the β-hairpin structural element.

Previously, we have shown that peptide fragments from an antibody can be used as antiviral lead structures and further optimized by computational approaches (Memczak et al. 2016). Beyond that, multivalent peptide-conjugate nanoparticles can improve antiviral effects even more (Lauster et al. 2017; Mesias et al. 2021).

Several ACE2-derived peptides, most of which are variations of the ACE2 helix-1 (see Figure 1) designed to improve helical content in solution, have been shown to competitively inhibit the SARS-CoV-2 spike protein attachment to its receptor (Curreli et al. 2020; Karoyan et al. 2021). The extended β-hairpin segment of p6 permits this peptide to form additional interactions with the RBD, specifically with ACE2 residue K353. Not only has the single point mutation K353A been shown to abolish the interaction with the RBD of SARS-CoV-2 (Wang et al. 2020a), but also several SARS-CoV-2 variants, namely those with the N501Y mutation, display enhanced interactions with K353 (Gan et al. 2021; Verma and Subbarao 2021; Zhu et al. 2021). Recently, a short peptide containing seven residues of the same β-hairpin was found to bind the SARS-CoV-2 spike RBD with nM affinity (Han et al. 2021).

Here, we report the binding affinity of both p4 and p6 to the SARS-CoV-2 RBD. Using a combined computational-experimental approach, we identify key anchor residues in the peptide-RBD interaction and evaluate variants designed

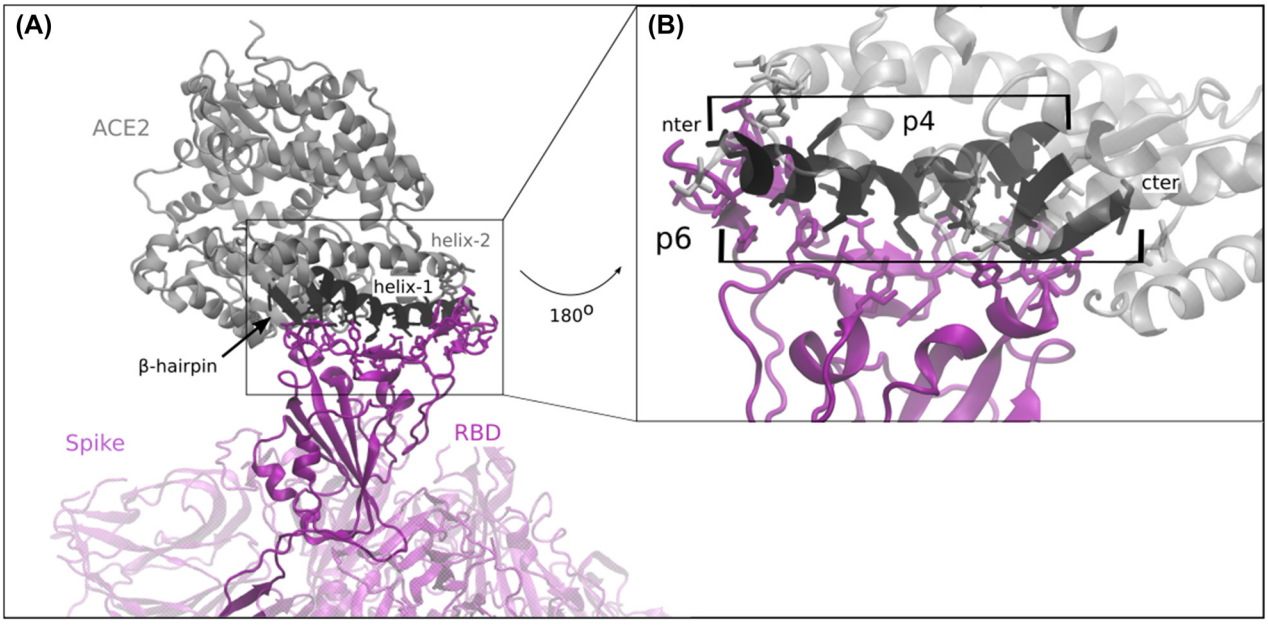

Figure 1: Schematic representation of ACE2-RBD interaction.
(A) CryoEM structure of the complex of human ACE2 (gray) with SARS-CoV-2 RBD of the viral S-protein (purple, PDB:7DF4). The RBD is highlighted (dark purple) and the key residues for the interaction with the ACE2 (SI Table 2) are represented as sticks. Helix-1 and the β-hairpin of ACE2 are shown in black, and key residues for the interaction with the RBD are represented as sticks. (B) Zoom in of the ACE2-RBD interface, and 180° rotation for better visualization. Antiviral ACE2-derived peptides p4 and p6 are marked.

to further enhance specific interactions with the SARS-CoV-2 RBD or improve peptide helicity. Our results support the notion that extension of the peptide could enhance key interactions, however the stabilization of the peptide secondary structure is indispensable for improved binding. Therefore, we further demonstrate that peptide cyclization is a promising strategy for achieving this stabilization.

Results

Binding affinity of p4 and p6 towards SARS-CoV-2 RBD

We measured the K_D value for p4 and p6 to the RBD of wild-type SARS-CoV-2 using microscale thermophoresis (MST), and we obtained dissociation constants of 0.93 ± 0.21 μM and 0.45 ± 0.09 μM, respectively (Figure 2A). These results are consistent with the ones obtained from measurements with SARS-CoV-1, showing an increased antiviral activity for p6 compared to p4 indicating a stronger interaction with the RBD (Han et al. 2006). Similar values were also obtained for RBD variants alpha and delta (Supplementary Information, Table 1 and SI Figure 1), showing the broad inhibitor potential for these peptides. We thus studied p6, which is only seven ACE2 residues longer than p4 but shows a doubled binding affinity. Likewise, in a recent work we reported the interaction of recombinant ACE2 and the RBD to be in the same range (Nie et al. 2021), also similar to values found in the literature (Barton et al. 2021; Chan et al. 2020; Lan et al. 2020).

Despite its increased affinity in comparison to p4, the affinity of p6 to the RBD is still approximately half an order of magnitude lower than that of ACE2 for the RBD. Interestingly, the helical content decreases with the C-terminal extension, as shown by comparing the helicity of p4 with p6. This effect is intensified by dissolving the peptides in TFE (Figure 2B and C). To gain further insight into the p6-RBD complex with the intention of proposing variants with enhanced binding, we performed all-atom Molecular Dynamics (MD) simulations of the complex, starting from the ACE2-RBD cryoEM structure (PDB: 7DF4) (Xu et al. 2021). During the simulations we observed that the structure of p6 fluctuates substantially from the bioactive conformation (i.e., the corresponding peptide regions within ACE2 bound to the RBD). This large conformational flexibility can be observed in the multimodal distribution of the root mean square deviation (RMSD) of the MD-configurations from the initial structure (Figure 3A). We calculated the per-residue contribution to binding by using the molecular mechanics energies with a generalized Born and surface area continuum solvation method (MM/GBSA) (Figure 3B). The average value of the binding enthalpy for the complex was −35 ± 4 kcal/mol. We noted that the truncation of the RBD-interacting interface of

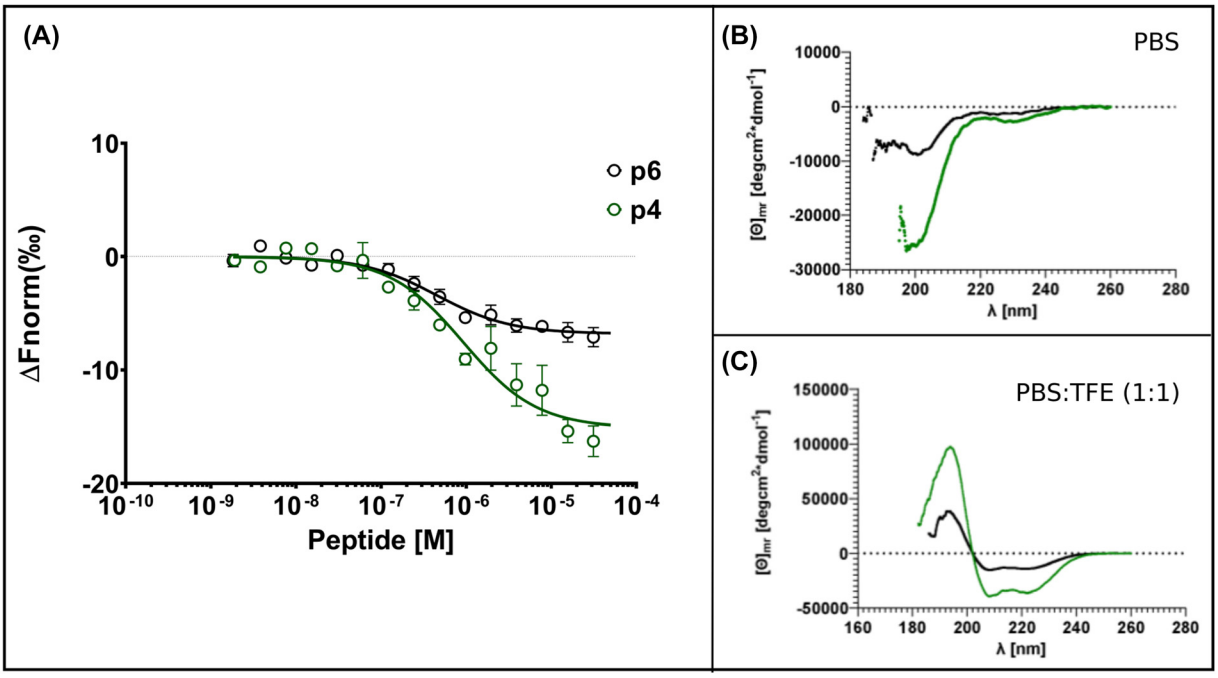

Figure 2: Affinity and structural characterization of ACE2-derived peptides.
(A) MST binding curves from experiment using different concentrations of ACE2-derived peptides p4, p6 against constant concentration of fluorescently labeled RBD. Error bars: SEM with $N = 3$. (B) CD spectra for peptides p4 and p6, acquired in 20 mM phosphate buffer, and (C) in presence of 50% of trifluoroethanol as an helicity inducer.

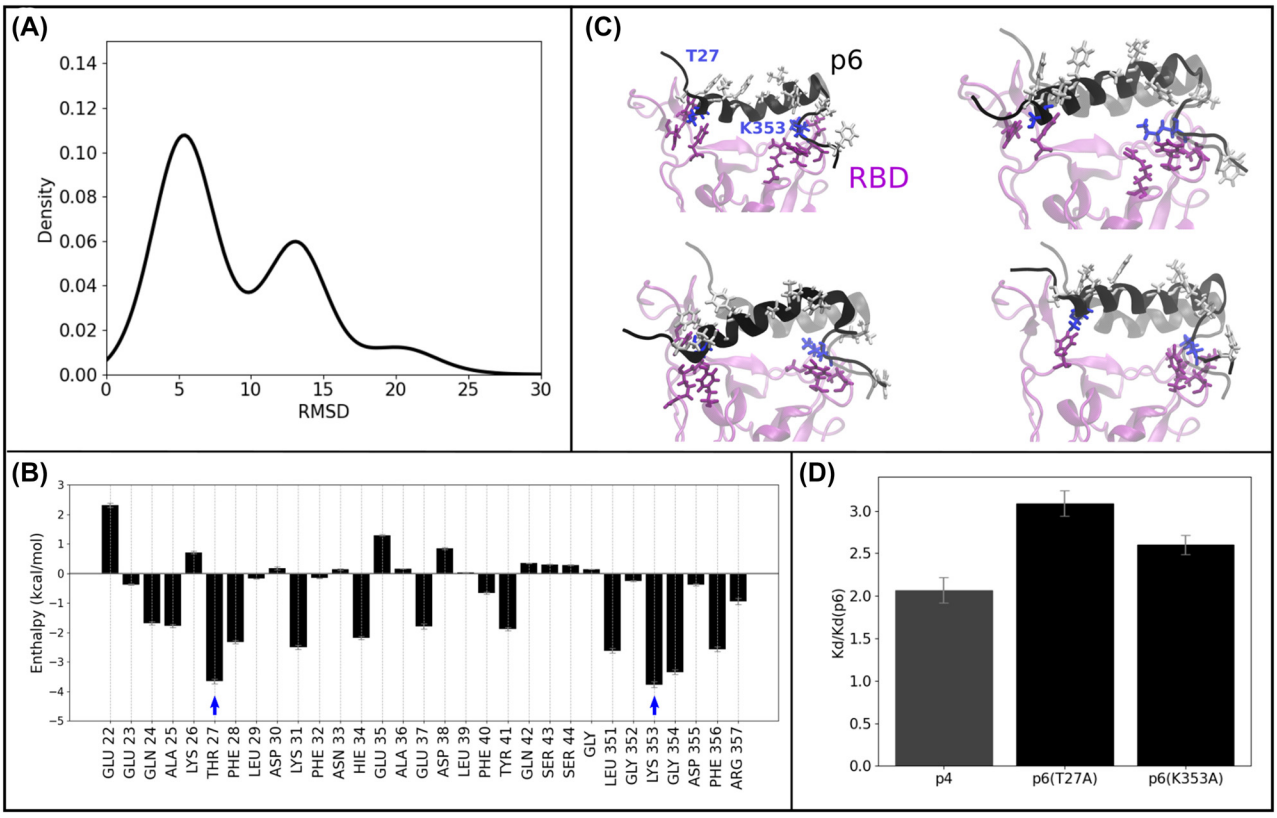

Figure 3: Analysis of SARS-CoV-2 RBD-p6 complex stability.
(A) Density plot of RMSD p6 residues (estimated by considering peptide backbone positions after concatenating three independent 250-ns MD simulations). (B) Per-residue contributions to the binding enthalpy and error bars show average and confidence interval (95%) from three replicas concatenated into a single trajectory. Overall binding energy of the complex is −34.8 ± 0.7 kcal/mol. Blue arrows highlight the two anchor residues T27 and K353. (C) Snapshots of p6 (black) bound to the RBD (purple), from MD simulations are shown as ribbons with the initial structure of p6 superimposed in gray. Solvent-exposed hydrophobic amino acids are shown as white sticks. The anchors are shown as blue sticks and RBD residues within 3 Å from the anchors as purple sticks. (D) K_D^X/K_D^{p6} ratios obtained from MST experiments are shown, where X is either p4, p6(T27A) or p6(K353A) and error bars show the standard deviation. Absolute K_D values are provided in SI Table 3.

ACE2 results in the disruption of hydrophobic interactions, leaving some hydrophobic residues exposed to the solvent, consequently destabilizing the overall peptide secondary structure in solution (Figure 3C).

Despite the variable observed binding modes of p6, two residues, T27 and K353, stand out in respect to the number of contacts established during the simulations of the complex, which is also reflected in their favorable per-residue energy contributions (Figure 3B). To further evaluate the specific anchoring roles of T27 and K353, we synthesized p6 single point alanine mutants T27A and K353A and evaluated their affinities for the RBD using MST (SI Figure 4). The dissociation constants for each of the mutants is comparable to that of p4, indicating a 3-fold loss in affinity relative to p6 due to the deletion of the 7-residue β-hairpin segment, or one of the two anchor residues alone (Figure 3D).

Analysis of p6 variants

In an attempt to design ACE2-derived peptides with antiviral activity against SARS-CoV-2 we used p6 as a lead structure peptide and evaluated five variants, denoted p6A to p6E (aligned sequences shown in Figure 4A). p6A and p6B contain mutations of several hydrophobic and non-interacting residues (i.e., residues that participate in native intramolecular ACE2 hydrophobic contacts); the former also incorporates one mutation (E22Y) to favor new interactions and the latter had two additional N-terminal residues, included to promote the stabilization of its α-helix (Petukhov et al. 2009). In variants p6C-E, we aimed at enhancing favorable peptide-RBD interactions by extending the N-terminal region with wild-type (WT) residues from ACE2 helix-2, using two residues from helix-1 to artificially link these two segments (Figure 4B); in particular p6C is the WT

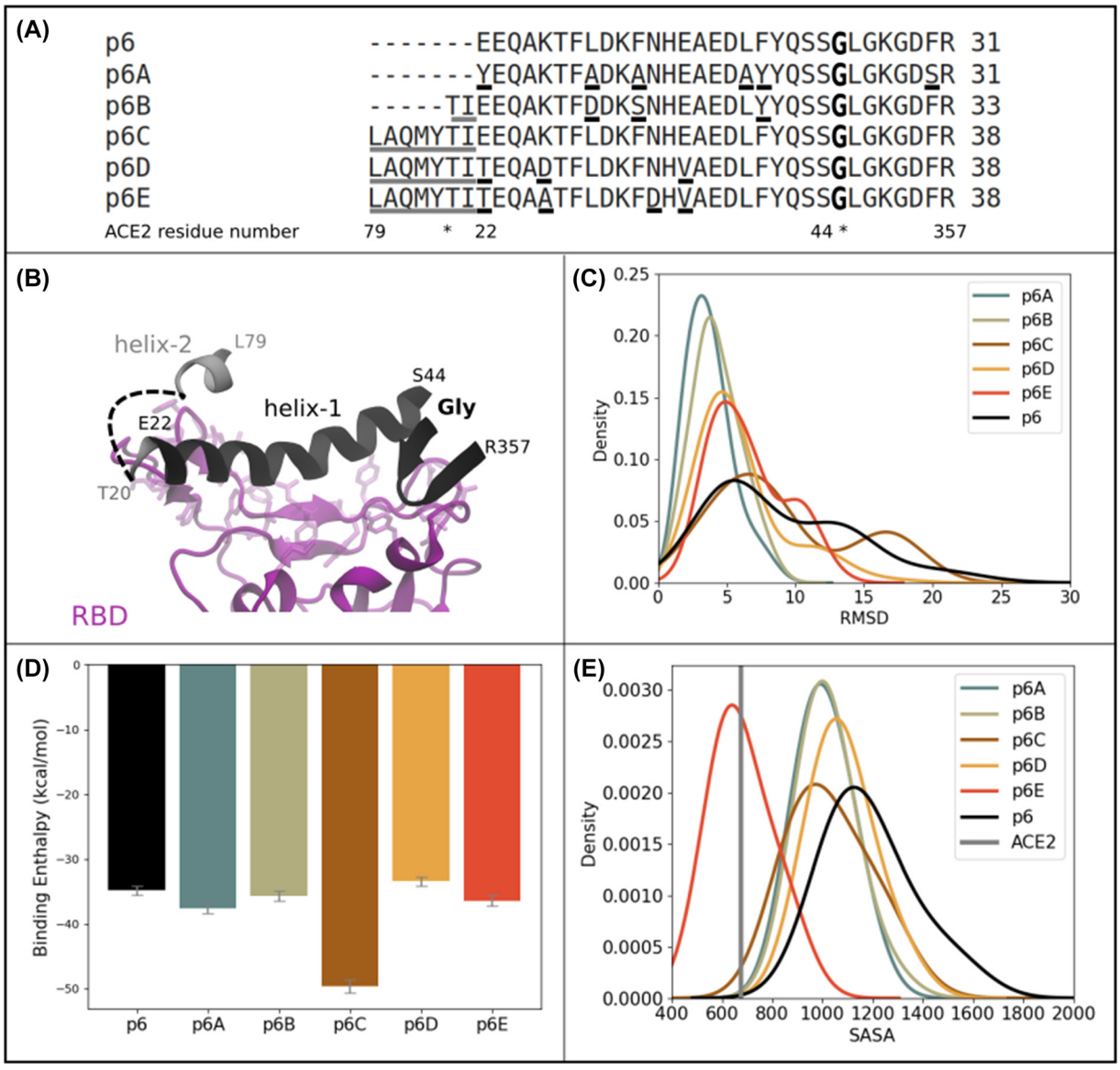

Figure 4: Characterization of p6 and variants thereof in complex to the RBD.
(A) Aligned sequences of p6 and p6 variants (Madeira et al. 2019). The black underline represents mutations and the gray underline represents the addition of residues. Some ACE2 residue numbers are shown as a reference. Non-consecutive regions are pointed out with an asterisk. The glycine in bold was added artificially and it is not within the ACE2. (B) ACE2-RBD interface with the RBD shown as purple cartoon and p6 shown as black cartoon. The position of the glycine that joins ACE2 helix-1 and the β-hairpin is highlighted. Residues added to p6B and to p6C, D, E are shown in gray cartoons. The gray-dashed line represents the junction made for p6C, D and E. Some ACE2 residue numbers are shown as a reference. (C) Density plot of p6 and p6 variants RMSD residues. (D) Binding enthalpies of p6 and p6 variants and error bars show average and standard error of the mean from three replicas concatenated into a single trajectory for each system. (E) Density plot of solvent surface accessible area (SASA) for key RBD residues. The gray straight line represents SASA for the key RBD residues (as defined in SI Table 2) in the CryoEM structure of the complex RBD:ACE2 (PDB:7DF4).

sequence with just this N-terminal extension, whereas p6D and p6E have the same length but with further punctual mutations intended to enhance intermolecular interactions. An ACE2 mutational analysis recently reported was taken into consideration in proposing these specific mutations (Chan et al. 2020).

We performed MD simulations of each variant bound to the RBD, so as to compare their structural stability and binding affinity. The RBD structure remained stable in all simulations and the RMSD of the backbone atoms remained below 3.5 Å during the three 250-ns trajectories (SI Figure 2A). The RMSF of the RBD residues (SI Figure 2B)

presented a region with more fluctuations (T470-F490) which corresponds to a mobile loop that has been reported to enhance interactions in SARS-CoV-2 compared to SARS-CoV-1 (Wang et al. 2020a; Xu et al. 2021). The N-terminal region of ACE2 and some residues from helix-2 interact with this loop. We note that the three extended variants (p6C, p6D, and p6E) include this RBD binding region, whereas p6A and p6B do not (Figure 4A). The distributions of RMSD values for the five variants indicate that all maintained the initial bioactive conformation better than the WT p6 sequence, with the exception of p6C, which was similar to p6 in terms of its overall flexibility (Figure 4C). The estimated binding enthalpies, in contrast, showed only slight improvements in binding, and only for p6C (Figure 4D). Not only the helix formation is strongly hindered without the ACE2 context, but also the β-hairpin. During the MD runs, p6 maintains residues 351, 352, 355, 356, 357 on an antiparallel β-strand structure, as in the ACE2, 22% of the time on average, p6D and p6E about 10%, and p6A, B and C less than 5% (SI Figure 2C).

Keeping in mind that the goal of designing peptides requires they competitively inhibit ACE2-RBD binding, we considered how well the different binding modes of the variants covered residues known to be involved in the ACE2-RBD interaction. Figure 4E shows the distribution of the total solvent accessible surface area (SASA) of critical RBD residues (SI Table 2) from the combined 750-ns simulation of each variant. In the native bioactive conformation, the corresponding SASA value is approximately 700 $Å^2$ (gray reference line in Figure 4E), reflecting the tightly bound ACE2-RBD complex. As the distribution of SASA values shifts closer to this reference line, we consider the variant binding mode(s) to be more effective at "covering" the critical portions of the RBD. The analysis of the SASA distributions shows that all variants of p6 are slightly shifted to the left with respect to the WT p6 sequence, with p6E particularly standing out in this regard.

Together these analyses highlight that the mutation of solvent-exposed hydrophobic residues appears to be most effective at stabilizing the bound conformation of p6 variants (p6A and p6B, Figure 4C), whereas the extension of the N-terminal region showed more of an impact in enhancing the coverage of important RBD residues (in particular p6E, Figure 4E) and in enhancing the calculated total binding enthalpy (variant p6C, Figure 4D).

Based on the above computational analyses of the peptide-RBD simulations, p6D was excluded for the experimental characterization because neither the binding energy of the complex nor the coverage of key RBD residues was enhanced. Even though the binding enthalpies of p6A and p6B to the RBD did not show improvement with respect to p6, both showed promise in terms of conformational stability in the bioactive conformation (Figure 4C) and coverage of key RBD residues (Figure 3E).

We synthesized and characterized p6A, p6B, p6C and p6E by CD spectroscopy and evaluated affinity for the SARS-CoV-2 spike RBD using MST measurements. All peptides were soluble until a 0.25 mM concentration in physiological phosphate buffer at room temperature and the peptide solutions were translucent along the concentrations evaluated in the MST experiments. The helicity in trifluoroethanol (TFE) was lower than that of p6 for all the variants and the binding affinity did not have an improvement compared to p6 (Figure 5, see also SI Table 3). Nevertheless, we observed that variants with higher helical content had higher affinities to the RBD, with the logical exception of the single-point alanine substitutions of the anchor residues.

To further explore the hypothesis that a stabilization of the α-helical structure could enhance peptide-RBD binding, we designed a cyclized p6 variant, denoted p6-cyc. Starting from p6 sequence, we replaced A36 for Fmoc-(R)-2-(7-octenyl)Ala-OH, and S43 for Fmoc-(S)-2-(4-pentenyl)Ala-OH, and subsequently performed Ring Closing Metathesis (RCM) as described in supplementary information. The positions selected for RCM implied substitution of aliphatic amino acids that were not important for the interaction with the RBD with an adequate distance in the peptide sequence to reach a (i, i+7) type of stapling. The cyclized peptide effectively not only showed a higher helical content in TFE, but also a 25% helical content in buffer, and in accordance with our hypothesis this translated with a slightly better affinity towards the spike protein RBD, as demonstrated by

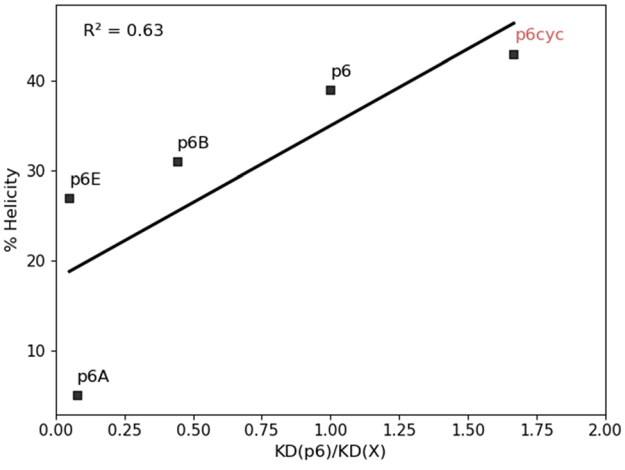

Figure 5: K_D^{p6}/K_D^X ratios obtained from MST experiments with respect to the % helical content measured from CD spectra of peptides in PBS:TFE (1:1) solution. P6-cyc is highlighted in red.

MST experiments. This indicates that peptide cyclization is a promising strategy to incorporate into antiviral peptide design efforts, as also described in other approaches for other systems (Curreli et al. 2020; Maas et al. 2021; Morgan et al. 2021).

Discussion

Here we present a study of the interaction between ACE2-derived peptides and the RBD of SARS-CoV-2 using a combined experimental and theoretical approach. Beginning with two peptides, p4 and p6, both of which were previously proposed for SARS-CoV-1 as potential antivirals, we designed variants of p6 with the goal of improving peptide-RBD binding and further understanding the driving factors underlying this molecular recognition.

Our results show that p6 has a three-fold higher affinity for the SARS-CoV-2 RBD than p4, which is consistent with the previously reported trend in the two peptides' differential antiviral activity for SARS-CoV-1. Using molecular dynamics simulations, we evaluated the conformational stability and binding enthalpy of the p6-RBD complex, where we observed the conformational plasticity of p6. The per-residue contributions to the binding enthalpy highlight two residues of p6, T27 and K353, that act as anchors in the peptide-RBD complex. T27 establishes critical hydrophobic interactions with many RBD residues (L455, F456, Y473, A475 and Y489, as denoted in SI Table 2, conserved in all tested RBD variants). Interestingly, the key interactions provided by K353 and their counterparts G496, Q498, G502 and Y505 (conserved in all RBD variants) is located on the 7-residue β-hairpin that distinguishes p6 from p4. Furthermore, we observed that the single point mutant K353A reduces the K_D of p6 by a factor of three, making it comparable to that of p4. Interestingly, in the recently appeared Omicron variant presenting 15 mutations in the RBD (Mannar et al. 2022), all these interactions seem to be conserved as most key residues interacting with T27 or K353 are not mutated, reinforcing the idea that these anchors seem critical to ensure ACE2 recognition, and thus the potential inhibitory effect of the ACE2-derived peptides. However, with the emergence of new variants of SARS-CoV-2, the expected efficacy of ACE2-derived peptides in light of the mutations in the RBD should be evaluated in each case.

Based on these analyses of the p6-RBD complex, we proposed variants of p6 with the underlying assumption that the bioactive conformation of the ACE2-derived peptide bound to the RBD would be similar to that of the corresponding segments in the ACE2-RBD structure. Indeed MD simulations indicated that all designed variants were more stable in the bioactive conformation than WT p6. The most drastic change explored in the variants was the extension of the N-terminal region to further include the so-called ACE2-hydrophobic patch. This ACE2-hydrophobic patch, which also contains the proposed anchor T27, was found to be the last residue detaching from the RBD during the dissociation process as previously reported MD simulation work (Taka et al. 2021). Our results show that this N-terminal extension alone (variant p6C) resulted in an enhanced binding enthalpy. The stabilization of the β-hairpin structure could be another strategy in search of binding improvement as the other anchor, K353, sits at its very loop tip. Such stabilization could be achieved by means of specific click cyclization (Park and Waters 2013), acyclic scaffold (Stanojlovic et al. 2022), or other methodology that warrants the position of the residues in the β-hairpin conformation, resembling the ACE2 structure.

In sharp contrast to the MD results, the experimental characterization by CD spectroscopy of the peptides in solution showed that they do not present a stable α-helix structure in fully aqueous solution, though after the addition of TFE, all peptides presented a fraction of helicity. This result indicates that the underlying assumption regarding the conservation of the bioactive conformation in all peptide variants cannot be supported, and the enhanced binding enthalpies calculated likely reflect this finding as a result of starting the simulations in the bioactive/bound conformation.

Though none of the five initially designed variants showed improved affinity for the RBD, we did observe a correlation between the fraction of helical content and the respective K_D values, which led to the hypothesis that if the peptide structure were sufficiently constrained, RBD binding could be improved. To support this hypothesis, we designed a cyclized variant of p6, p6-cyc, which enhances peptide helicity and the RBD binding affinity in a linear proportional manner. Moreover, MD simulations of p6-cyc and p6A-E in a cyclic form could be another step forward in finding effective ACE2-derived peptides.

We showed that the C-terminal segment of p6 together with an extension of the N-terminal region resembling the helix-2 of the ACE2 can be a promising peptide that could bind the RBD efficiently mimicking the ACE2, but the challenge will be to warrant the secondary structure stability in solution. Our results show that peptide cyclization is likely an effective strategy to include for this design purpose. Furthermore, a multivalent presentation of ACE2 derived and engineered peptides can lead to even higher affinity binders, as trimeric or even multiple interactions with one or more trimeric spike proteins of SARS-CoV-2 can be formed. Further, such nanoparticles also add a steric

inhibition component, provided by the scaffold, which can decrease the infection inhibition concentration beyond the affinity value (Bhatia et al. 2017; Lauster et al. 2017).

Materials and methods

Systems preparation for MD simulations

Six ACE2-derived peptides (p6 and five variants named as p6A-E) were simulated and analyzed in complex with wild-type SARS-CoV-2 RBD (residues 319 to 541). The initial configuration of all systems were taken from 7DF4 PDB [7DF4.pfb]. p6 was constructed by truncating ACE2 from residues 22 to 44 and 351 to 357. A glycine was added between the two non-consecutive parts of p6. p6A is a p6-mutated peptide as well as p6B, but the latter also has two more residues from the α-helix, 20 and 21. p6C is an extended version compared to p6 and it was designed based on p6 structure with the addition of ACE2 residues 79 to 83 at the N-terminal. In order to fill the gap between residues 83 and 22 (Figure 4B), residues 20 and 21 were artificially moved between residues 83 and 22, allowing the correct joint of these other non-consecutive parts. Therefore, p6 and p6C peptides present no mutations from the wild-type structure, but spatial rearrangements and the addition of the above-mentioned Gly. As p6D and p6E are also extended peptides, they were prepared with the same protocol as p6C. The RBD residues taken from the PDB structure were 319–541 from the monomer in the up-conformation (chain B).

The protonation state of ionizable residues were fixed to be those most probable at neutral pH, after estimation of side chain pKa values with propka 3.0, an empirical pKa predictor for buried and surface protein residues (Olsson et al. 2011). All of the His residues were determined to be protonated solely at the Nε (HIE).

All systems were modeled with the Amber ff14SB force field (Maier et al. 2015). All systems were solvated with the TIP3P water model (Jorgensen et al. 1983) using the tLeAP module of the Amber simulation suite, in octahedral boxes using a distance of 10 Å from the protein surface, resulting in the addition of approximately 25,000 TIP3P residues for the systems, respectively. A physiological salt concentration of 0.15 M was achieved through the addition of approximately 70 Na^+ and Cl^- ions, respectively, after neutralizing the system charge in each case (p6: −3e; p6A: −4e; p6B: −2e; p6C: −3e; p6D: −3e; p6E: −3e; RBD has +7e additional charge for the complex). Hydrogens and other atoms not resolved in the cryo EM structures, as well as the disulfide bonds (UniProt Consortium 2021), were added using the tLeAP module of the Amber simulation suite (Case et al. 2021).

MD simulations production and analysis protocols

Each system had an initial energy minimization, heating from 0 to 200 K over 50 ps with a 1 fs time step with strong restraints (100 kcal/mol/Å^2) on the protein, and then heating from 200 to 300 K under the same conditions with weaker restraints on the protein (50 kcal/mol/Å^2). The system was then equilibrated for an additional 50 ps at constant temperature and volume, without restraints, and finally at constant temperature and pressure without restraints for 50 ps. For constant pressure simulations, isotropic position scaling was performed with the Berendsen barostat and a pressure relaxation time of 2.0 ps. The Langevin thermostat was used with a collision frequency of 1.0 ps^{-1} (Sindhikara et al. 2009; Uberuaga et al. 2004). The SHAKE algorithm was used to constrain bonds to nonpolar hydrogens (Ryckaert et al. 1977). An 8.0-Å cutoff was used for nonbonded interactions.

For each complex, three replicas of 250 ns, under the same NVT conditions described above, with a 2.0 fs timestep, using the PMEMD cuda module of the Amber simulation suite (Case et al. 2021).

Trajectory analysis was performed using the CPPTRAJ module of the Ambertools 19 package of programs. The binding energy was computed from the first 200 ns of the molecular dynamics trajectories extracting snapshops with a 0.2 ns timestep, using the MM-GBSA (molecular mechanics, general-Born surface area) approach implemented in AMBER. The binding energy, ΔEbind,solv, was calculated as the sum of the terms:

$$\Delta Ebind, solv = \Delta Ebind, vacuum + \Delta Esol, complex - \Delta Esol, peptide + \Delta Esol, protein$$

where ΔEbind,vacuum corresponds to the substrate binding energy in vacuum and ΔEsolv is the corresponding energy for the solvation process of each species. We performed an energy decomposition for the protein residues involved in interactions with the peptide. For the Solvent-Accessible Surface Area (SASA), we first made a detailed analysis of the interactions observed between the ACE2 and the RBD (Figure 1, SI Table 2). We compiled data already reported in the literature and calculated the SASA, using CPPTRAJ with a solvent-probe radius of 1.4 Å (Weiser et al. 1999), for the key RBD residues involved: 417, 446, 449, 453, 455, 456, 473–476, 474, 475, 476, 484, 486–490, 493–496, 498, 500–502, 505 (Lan et al. 2020; Wang et al. 2020a, 2020b; Xu et al. 2021; Yan et al. 2020). We estimated the per-residue average of antiparallel β-strand structure with the CPPTRAJ module of the AmberTools package.

Peptide synthesis, purification and characterization

All the peptides were synthesized on Rink Amide using automated SPPS standard protocols. For the cyclized version of p6, stapling was performed on a resin following known methodologies for ring closing metathesis: the resin was incubated with a 10 mM solution of bis(tricyclohexylphosphine)-benzylidene ruthenium (IV) (1st generation Grubb's catalyst) in 1,2-dichloroethane for 1 h twice. In all the cases, the peptide cleavage from the resin was performed using a 95:2.5:2.5 mixture of TFA:water:TIPS. Subsequent purification was performed on prepHPLC systems using C18 chromatographic columns, with different mixtures of water:acetonitrile, and after lyophilization peptides were obtained as pure white powders, their purity being determined by 15 min chromatography runs on a C18 UPLC-MS instrument. Characterization was mainly done by determining helical content by circular dichroism spectra, and high resolution mass spectrometry of the pure samples (SI Figures 6–23).

Peptide binding affinity measurements

For affinity measurements His-tagged RBD of the wild-type SARS-CoV-2 (2019-nCoV) S-protein from recombinant expression in mammalian cells was kindly provided by Dr. Coskun (Technical University Dresden,

Germany). S-protein RBD variants alpha (B.1.1.7) and delta (B.1.617.2) were provided from SinoBiological.

RBD labeling and purification was performed using a 2nd generation NHS-Red labeling kit (NanoTemper). RBD solution was diluted with water to 10 μM, rebuffered in sodium carbonate aqueous solution at pH 8.0, and incubated in the dark at 300 μM of the red dye. Size exclusion chromatography allowed to obtain the labeled RBD free of unreacted dye. The labeling efficiency was analyzed from spectroscopy measurements to be approximately 1:1 (protein:dye). Affinity measurements were conducted in DPBS (without Ca^{2+} and Mg^{2+}) supplemented with 0.05% (v/v) Tween20, and premium capillaries (NanoTemper).

Microscale thermophoresis (MST) was then measured by making 16 sequential 1:1 dilutions of each peptide, using PBS + 0.05% Tween 20 as diluent, each with a final volume of 10 μL. Each diluted sample was then incubated with 10 μL of the 10 nM labeled RBD stock solution, therefore always keeping a 5 nM concentration of the labeled target protein in every sample.

MST signal was then acquired in a NanoTemper Technologies Monolith NT.115 Pico instrument, at an excitation power of 20% and a MST power of 40%, the signal was analyzed 1.5 s after the start of the IR-laser, and the obtained data fitted as shown previously (Bhatia et al. 2017). These conditions were kept the same for all the measured samples. All measurements were done at least by triplicate (SI Figures 3–5).

Acknowledgments: We acknowledge computational resources granted by INQUIMAE-CONICET (cluster Logan) and Facultad de Ciencias Exactas y Naturales, Universidad de Buenos Aires (cluster CECAR). We further acknowledge the laboratory of Dr. Coskun (TU Dresden) for providing us recombinant RBD of wild-type SARS-CoV-2, and technical assistance from AG Hackenberger – FMP Berlin.

Author contributions: All the authors have accepted responsibility for the entire content of this submitted manuscript and approved submission.

Research funding: This work was funded by the Berlin University Alliance (BUA; Corona Virus Pre-Exploration Project), and the Federal Ministry of Education and Science (BMBF; grant number: 13XP5111). S.D.L. and M.A. are members of the research career at the Argentinean National Research Council CONICET. C. Sarto is supported by a CONICET graduate fellowship.

Conflict of interest statement: The authors declare no conflicts of interest regarding this article.

References

Barton, M.I., MacGowan, S.A., Kutuzov, M.A., Dushek, O., Barton, G.J., and van der Merwe, P.A. (2021). Effects of common mutations in the SARS-CoV-2 Spike RBD and its ligand, the human ACE2 receptor on binding affinity and kinetics. eLife 10, https://doi.org/10.7554/eLife.70658.

Bhatia, S., Lauster, D., Bardua, M., Ludwig, K., Angioletti-Uberti, S., Popp, N., Hoffmann, U., Paulus, F., Budt, M., Stadtmüller, M., et al. (2017). Linear polysialoside outperforms dendritic analogs for inhibition of influenza virus infection in vitro and in vivo. Biomaterials 138: 22–34.

Brielle, E.S., Schneidman-Duhovny, D., and Linial, M. (2020). The SARS-CoV-2 exerts a distinctive strategy for interacting with the ACE2 human receptor. Viruses 12: 497.

Case, D.A., Metin Aktulga, H., Belfon, K., Ben-Shalom, I., Brozell, S.R., Cerutti, D.S., Cheatham, T.E., III, Cruzeiro, V.W.D., Darden, T.A., Duke, R.E., et al. (2021). *Amber 2021*. San Francisco, USA: University of California.

Chan, K.K., Dorosky, D., Sharma, P., Abbasi, S.A., Dye, J.M., Kranz, D.M., Herbert, A.S., and Procko, E. (2020). Engineering human ACE2 to optimize binding to the spike protein of SARS coronavirus 2. Science 369: 1261–1265.

Curreli, F., Victor, S.M.B., Ahmed, S., Drelich, A., Tong, X., Tseng, C.-T.K., Hillyer, C.D., and Debnath, A.K. (2020). Stapled peptides based on human angiotensin-converting enzyme 2 (ACE2) potently inhibit SARS-CoV-2 infection. mBio 11: e02451-20.

Dodero-Rojas, E., Onuchic, J.N., and Whitford, P.C. (2021). Sterically confined rearrangements of SARS-CoV-2 spike protein control cell invasion. eLife 10: e70362.

Fan, X., Cao, D., Kong, L., and Zhang, X. (2020). Cryo-EM analysis of the post-fusion structure of the SARS-CoV spike glycoprotein. Nat. Commun. 11: 3618.

Gan, H.H., Twaddle, A., Marchand, B., and Gunsalus, K.C. (2021). Structural modeling of the SARS-CoV-2 spike/human ACE2 complex interface can identify high-affinity variants associated with increased transmissibility. J. Mol. Biol. 433: 167051.

Han, D.P., Penn-Nicholson, A., and Cho, M.W. (2006). Identification of critical determinants on ACE2 for SARS-CoV entry and development of a potent entry inhibitor. Virology 350: 15–25.

Han, S., Zhao, G., Wei, Z., Chen, Y., Zhao, J., He, Y., He, Y.-J., Gao, J., Chen, S., Du, C., et al. (2021). An angiotensin-converting enzyme-2-derived heptapeptide GK-7 for SARS-CoV-2 spike blockade. Peptides 145: 170638.

Hoffmann, M., Kleine-Weber, H., Schroeder, S., Krüger, N., Herrler, T., Erichsen, S., Schiergens, T.S., Herrler, G., Wu, N.-H., Nitsche, A., et al. (2020). SARS-CoV-2 cell entry depends on ACE2 and TMPRSS2 and is blocked by a clinically proven protease inhibitor. Cell 181: 271–280.e8.

Jorgensen, W.L., Chandrasekhar, J., Madura, J.D., Impey, R.W., and Klein, M.L. (1983). Comparison of simple potential functions for simulating liquid water. J. Chem. Phys. 79: 926–935.

Karoyan, P., Vieillard, V., Gómez-Morales, L., Odile, E., Guihot, A., Luyt, C.-E., Denis, A., Grondin, P., and Lequin, O. (2021). Human ACE2 peptide-mimics block SARS-CoV-2 pulmonary cells infection. Commun. Biol. 4: 197.

Kirchdoerfer, R.N., Wang, N., Pallesen, J., Wrapp, D., Turner, H.L., Cottrell, C.A., Corbett, K.S., Graham, B.S., McLellan, J.S., and Ward, A.B. (2018). Stabilized coronavirus spikes are resistant to conformational changes induced by receptor recognition or proteolysis. Sci. Rep. 8: 15701.

Lan, J., Ge, J., Yu, J., Shan, S., Zhou, H., Fan, S., Zhang, Q., Shi, X., Wang, Q., Zhang, L., et al. (2020). Structure of the SARS-CoV-2 spike receptor-binding domain bound to the ACE2 receptor. Nature 581: 215–220.

Lauster, D., Glanz, M., Bardua, M., Ludwig, K., Hellmund, M., Hoffmann, U., Hamann, A., Böttcher, C., Haag, R., Hackenberger, C.P.R., et al. (2017). Multivalent peptide-nanoparticle conjugates for influenza-virus inhibition. Angew. Chem. Int. Ed. 56: 5931–5936.

Li, F. (2015). Receptor recognition mechanisms of coronaviruses: a decade of structural studies. J. Virol. 89: 1954–1964.

Maas, M.N., Hintzen, J.C.J., Löffler, P.M.G., and Mecinović, J. (2021). Targeting SARS-CoV-2 spike protein by stapled hACE2 peptides. Chem. Commun. 57: 3283–3286.

Madeira, F., Park, Y.M., Lee, J., Buso, N., Gur, T., Madhusoodanan, N., Basutkar, P., Tivey, A.R.N., Potter, S.C., Finn, R.D., et al. (2019). The EMBL-EBI search and sequence analysis tools APIs in 2019. Nucleic Acids Res. 47: W636–W641.

Maier, J.A., Martinez, C., Kasavajhala, K., Wickstrom, L., Hauser, K.E., and Simmerling, C. (2015). ff14SB: improving the accuracy of protein side chain and backbone parameters from ff99SB. J. Chem. Theor. Comput. 11: 3696–3713.

Mannar, D., Saville, J.W., Zhu, X., Srivastava, S.S., Berezuk, A.M., Tuttle, K.S., Marquez, A.C., Sekirov, I., and Subramaniam, S. (2022). SARS-CoV-2 omicron variant: antibody evasion and cryo-EM structure of spike protein–ACE2 complex. Science 375: 760–764.

Memczak, H., Lauster, D., Kar, P., Di Lella, S., Volkmer, R., Knecht, V., Herrmann, A., Ehrentreich-Förster, E., Bier, F.F., and Stöcklein, W.F.M. (2016). Anti-hemagglutinin antibody derived lead peptides for inhibitors of influenza virus binding. PLoS One 11: e0159074.

Mesias, V.S.D., Zhu, H., Tang, X., Dai, X., Guo, Y., Liu, W., and Huang, J. (2021). Effective ACE2 peptide-nanoparticle conjugation and its binding with the SARS-Cov-2 RBD quantified by dynamic light scattering. Chem. Commun. 57: 6979–6982.

Morgan, D.C., Morris, C., Mahindra, A., Blair, C.M., Tejeda, G., Herbert, I., Turnbull, M.L., Lieber, G., Willett, B.J., Logan, N., et al. (2021). Stapled ACE2 peptidomimetics designed to target the SARS-CoV-2 spike protein do not prevent virus internalization. Pept. Sci.: e24217.

Nguyen, H.L., Lan, P.D., Thai, N.Q., Nissley, D.A., O'Brien, E.P., and Li, M.S. (2020). Does SARS-CoV-2 bind to human ACE2 more strongly than does SARS-CoV? J. Phys. Chem. B 124: 7336–7347.

Nie, C., Pouyan, P., Lauster, D., Trimpert, J., Kerkhoff, Y., Szekeres, G.P., Wallert, M., Block, S., Sahoo, A.K., Dernedde, J., et al. (2021). Polysulfates block SARS-CoV-2 uptake through electrostatic interactions. Angew. Chem. Int. Ed. 60: 15870–15878.

Olsson, M.H.M., Søndergaard, C.R., Rostkowski, M., and Jensen, J.H. (2011). PROPKA3: consistent treatment of internal and surface residues in empirical pKa predictions. J. Chem. Theor. Comput. 7: 525–537.

Park, J.H. and Waters, M.L. (2013). Positional effects of click cyclization on β-hairpin structure, stability, and function. Org. Biomol. Chem. 11: 69–77.

Peter, E.K. and Schug, A. (2021). The inhibitory effect of a coronavirus spike protein fragment with ACE2. Biophys. J. 120: 1001–1010.

Petukhov, M., Tatsu, Y., Tamaki, K., Murase, S., Uekawa, H., Yoshikawa, S., Serrano, L., and Yumoto, N. (2009). Design of stable α-helices using global sequence optimization. J. Pept. Sci. 15: 359–365.

Ryckaert, J.-P., Ciccotti, G., and Berendsen, H.J.C. (1977). Numerical integration of the cartesian equations of motion of a system with constraints: molecular dynamics of n-alkanes. J. Comput. Phys. 23: 327–341.

Sindhikara, D.J., Kim, S., Voter, A.F., and Roitberg, A.E. (2009). Bad seeds sprout perilous dynamics: stochastic thermostat induced trajectory synchronization in biomolecules. J. Chem. Theor. Comput. 5: 1624–1631.

Stanojlovic, V., Müller, A., Moazzam, A., Hinterholzer, A., Ożga, K., Berlicki, Ł., Schubert, M., and Cabrele, C. (2022). A conformationally stable Acyclic β-hairpin scaffold tolerating the incorporation of poorly β-sheet-prone amino acids. Chembiochem 23: e202100604.

Taka, E., Yilmaz, S.Z., Golcuk, M., Kilinc, C., Aktas, U., Yildiz, A., and Gur, M. (2021). Critical interactions between the SARS-CoV-2 spike glycoprotein and the human ACE2 receptor. J. Phys. Chem. B 125: 5537–5548.

Uberuaga, B.P., Anghel, M., and Voter, A.F. (2004). Synchronization of trajectories in canonical molecular-dynamics simulations: observation, explanation, and exploitation. J. Chem. Phys. 120: 6363–6374.

UniProt Consortium (2021). UniProt: the universal protein knowledgebase in 2021. Nucleic Acids Res. 49: D480–D489.

Verma, J. and Subbarao, N. (2021). Insilico study on the effect of SARS-CoV-2 RBD hotspot mutants' interaction with ACE2 to understand the binding affinity and stability. Virology 561: 107–116.

Walls, A.C., Park, Y.-J., Tortorici, M.A., Wall, A., McGuire, A.T., and Veesler, D. (2020). Structure, function, and antigenicity of the SARS-CoV-2 spike glycoprotein. Cell 181: 281–292.e6.

Wang, Q., Zhang, Y., Wu, L., Niu, S., Song, C., Zhang, Z., Lu, G., Qiao, C., Hu, Y., Yuen, K.-Y., et al. (2020a). Structural and functional basis of SARS-CoV-2 entry by using human ACE2. Cell 181: 894–904.e9.

Wang, Y., Liu, M., and Gao, J. (2020b). Enhanced receptor binding of SARS-CoV-2 through networks of hydrogen-bonding and hydrophobic interactions. Proc. Natl. Acad. Sci. U.S.A. 117: 13967–13974.

Weiser, J., Shenkin, P.S., and Clark Still, W. (1999). Approximate atomic surfaces from linear combinations of pairwise overlaps (LCPO). J. Comput. Chem. 20: 217–230.

Wrapp, D., Wang, N., Corbett, K.S., Goldsmith, J.A., Hsieh, C.-L., Abiona, O., Graham, B.S., and McLellan, J.S. (2020). Cryo-EM structure of the 2019-nCoV spike in the prefusion conformation. Science 367: 1260–1263.

Xu, C., Wang, Y., Liu, C., Zhang, C., Han, W., Hong, X., Wang, Y., Hong, Q., Wang, S., Zhao, Q., et al. (2021). Conformational dynamics of SARS-CoV-2 trimeric spike glycoprotein in complex with receptor ACE2 revealed by cryo-EM. Sci. Adv. 7: eabe5575.

Yan, R., Zhang, Y., Li, Y., Xia, L., Guo, Y., and Zhou, Q. (2020). Structural basis for the recognition of SARS-CoV-2 by full-length human ACE2. Science 367: 1444–1448.

Zhao, P., Praissman, J.L., Grant, O.C., Cai, Y., Xiao, T., Rosenbalm, K.E., Aoki, K., Kellman, B.P., Bridger, R., Barouch, D.H., et al. (2020). Virus-receptor interactions of glycosylated SARS-CoV-2 spike and human ACE2 receptor. Cell Host Microbe 28: 586–601.e6.

Zhou, P., Yang, X.-L., Wang, X.-G., Hu, B., Zhang, L., Zhang, W., Si, H.-R., Zhu, Y., Li, B., Huang, C.-L., et al. (2020). A pneumonia outbreak associated with a new coronavirus of probable bat origin. Nature 579: 270–273.

Zhu, X., Mannar, D., Srivastava, S.S., Berezuk, A.M., Demers, J.-P., Saville, J.W., Leopold, K., Li, W., Dimitrov, D.S., Tuttle, K.S., et al. (2021). Cryo-electron microscopy structures of the N501Y SARS-CoV-2 spike protein in complex with ACE2 and 2 potent neutralizing antibodies. PLoS Biol. 19: e3001237.

Supplementary Material: The online version of this article offers supplementary material (https://doi.org/10.1515/hsz-2021-0426).